

# Bulk and wetting phenomena in a colloidal mixture of hard spheres and platelets

L. Harnau and S. Dietrich

*Max-Planck-Institut für Metallforschung, Heisenbergstr. 3, D-70569 Stuttgart, Germany,  
and Institut für Theoretische und Angewandte Physik,  
Universität Stuttgart, Pfaffenwaldring 57, D-70569 Stuttgart, Germany*

(Dated: November 5, 2018)

Density functional theory is used to study binary colloidal fluids consisting of hard spheres and thin platelets in their bulk and near a planar hard wall. This system exhibits liquid-liquid coexistence of a phase that is rich in spheres (poor in platelets) and a phase that is poor in spheres (rich in platelets). For the mixture near a planar hard wall, we find that the phase rich in spheres wets the wall completely upon approaching the liquid demixing binodal from the sphere-poor phase, provided the concentration of the platelets is smaller than a threshold value which marks a first-order wetting transition at coexistence. No layering transitions are found in contrast to recent studies on binary mixtures of spheres and non-adsorbing polymers or thin hard rods.

PACS numbers: 64.70.Ja, 68.08.Bc, 82.70.Dd

## I. INTRODUCTION

Rich bulk phase diagrams involving colloidal gas, liquid, and solid phases are found when non-adsorbing polymers or hard rodlike colloids are added as depletion agents to suspensions of colloidal spheres [1, 2]. The chemical potential of the polymers or rods, with which one can tune their concentration, plays a role equivalent to that of the inverse temperature for a simple one-component substance characterized by a soft pair potential. Moreover, it has been shown theoretically [3, 4] and by computer simulation [5] that entropic depletion mechanisms lead to interesting wetting phenomena and to a rich surface phase behavior in colloidal mixtures of spheres and non-interacting polymers or rods. A wetting transition and layering transitions have been found when the mixtures are exposed to a hard wall.

Recently the depletion potential between two hard spheres due to the presence of hard disclike colloids has been investigated [6, 7, 8, 9]. Subsequently it has been shown within of a free-volume theory that depletion induced phase separation in a colloidal sphere-platelet mixture should occur at low platelet concentrations in systems now experimentally available [10]. In view of the importance of such suspensions in biomedicine [11] and geophysics [12] we investigate in the present paper bulk and wetting phenomena of sphere-platelet mixtures using density functional theory. We demonstrate that the geometry-based density functional theory developed for binary mixture of hard spheres and thin rods [13, 14, 15, 16] can be consistently extended to the more challenging problem of hard spheres mixed with thin hard platelets (Sec. II). Moreover, we study the bulk phase diagram (Sec. III) and the wetting of the mixture at a planar hard wall by considering the platelets as thin and non-interacting regarding their mutual interactions (Sec. IV). Our study provides a direct comparison of the bulk and wetting properties of binary sphere-platelet and sphere-rod mixtures.

## II. DENSITY FUNCTIONAL AND FUNDAMENTAL MEASURE THEORY

We consider a binary mixture of hard spheres and thin circular platelets of radius  $R_s$  and  $R_p$ , respectively. The number density of the centers of mass of the platelets at a point  $\mathbf{r}$  with an orientation  $\omega_p = (\theta_p, \phi_p)$  of the normal of the platelets is denoted by  $\rho_p(\mathbf{r}, \omega_p)$  while  $\rho_s(\mathbf{r})$  is the center-of-mass number density of the spheres. The equilibrium density profiles of the inhomogeneous mixture under the influence of external potentials  $V_{ext,s}(\mathbf{r})$  and  $V_{ext,p}(\mathbf{r}, \omega_p)$  minimize the grand potential functional

$$\begin{aligned} \Omega[\rho_s, \rho_p] &= \int d^3r \rho_s(\mathbf{r}) [k_B T (\ln[\Lambda_s^3 \rho_s(\mathbf{r})] - 1) - \mu_s + V_{ext,s}(\mathbf{r})] \\ &\quad + \frac{1}{4\pi} \int d^3r d\omega_p \rho_p(\mathbf{r}, \omega_p) [k_B T (\ln[\Lambda_p^3 \rho_p(\mathbf{r}, \omega_p)] - 1) \\ &\quad - \mu_p + V_{ext,p}(\mathbf{r}, \omega_p)] + F_{ex}[\rho_s, \rho_p], \end{aligned} \quad (1)$$

where  $\Lambda_s, \Lambda_p$  are the thermal de Broglie wavelengths and  $\mu_s, \mu_p$  are the chemical potentials of the spheres and platelets, respectively. The spatial integrals run over the volume  $V$  which is accessible to the centers of the particles and  $\int d\omega = \int_0^\pi d\theta \int_0^{2\pi} d\phi$ . The excess free energy functional is obtained by integrating over an excess free energy density,

$$F_{ex}[\rho_s, \rho_p] = \frac{k_B T}{4\pi} \int d^3r d\omega_p \Phi(\{n_\nu^{(s)}, \mathbf{n}_i^{(s)}, n_\tau^{(p)}, n^{(sp)}\}), \quad (2)$$

where  $\nu = 0, 1, 2, 3$ ,  $i = 1, 2$ , and  $\tau = 0, 1, 2$ . In Eq. (2) the spatial and angular arguments of the weighted densities  $n_\nu^{(s)}, \mathbf{n}_i^{(s)}, n_\tau^{(p)}$ , and  $n^{(sp)}$  are suppressed in the notation. Here we use the following decomposition of the excess free energy density  $\Phi$ :

$$\Phi = \Phi_s + \Phi_{sp}, \quad (3)$$

with [17]

$$\begin{aligned} \Phi_s = & -n_0^{(s)} \ln(1 - n_3^{(s)}) + \frac{n_1^{(s)} n_2^{(s)} - \mathbf{n}_1^{(s)} \cdot \mathbf{n}_2^{(s)}}{1 - n_3^{(s)}} \\ & + \frac{(n_2^{(s)})^3 - 3n_2^{(s)} (n_2^{(s)})^2}{24\pi (1 - n_3^{(s)})^2}, \end{aligned} \quad (4)$$

and a new contribution

$$\begin{aligned} \Phi_{sp} = & -n_0^{(p)} \ln(1 - n_3^{(s)}) + \frac{n_1^{(p)} n^{(sp)} + n_1^{(s)} n_2^{(p)}}{1 - n_3^{(s)}} \\ & + \frac{\pi n_2^{(p)} (n_2^{(s)})^2}{64 (1 - n_3^{(s)})^2}. \end{aligned} \quad (5)$$

$\Phi_s$  is the original Rosenfeld excess free energy density [17] for a pure hard sphere fluid. (For the subtle issue of the range of validity of the Rosenfeld functional at high densities see Refs. [18, 19].)  $\Phi_{sp}$  takes sphere-platelet interactions into account up to first order in the number density of the platelets (see discussion below). There no is contribution  $\Phi_{pp}$  to the excess free energy  $\Phi$  in Eq. (4) because the platelets are considered as non-interacting particles regarding their mutual interactions. In the present application of density functional theory we concentrate on ordering effects induced by a planar hard wall such that the resulting density profile of the spheres depends on a single spatial variable  $z$  in the direction normal to the wall. Hence  $\rho_s(\mathbf{r}) = \rho_s(z)$  apart from possible surface freezing at high densities. Moreover, we assume invariance with respect to rotations around the  $z$  axis by an angle  $\phi_p$ , so that  $\rho_p(\mathbf{r}, \omega_p) = \rho_p(z, \theta_p)$ , where  $\theta_p$  is the angle between the normal of a platelet and the  $z$ -axis (see Fig. 1). In this planar geometry the weighted densities are given by

$$n_\nu^{(s)}(z) = \rho_s(z) \star w_\nu^{(s)}(z), \quad (6)$$

$$\mathbf{n}_i^{(s)}(z) = \rho_s(z) \star \mathbf{w}_i^{(s)}(z), \quad (7)$$

$$n_\tau^{(p)}(z, \theta_p) = \rho_p(z, \theta_p) \star w_\tau^{(p)}(z, \theta_p), \quad (8)$$

$$n^{(sp)}(z, \theta_p) = \rho_s(z) \star w^{(sp)}(z, \theta_p), \quad (9)$$

where the asterics  $\star$  denotes the spatial convolution:  $g(z) \star h(z) = \int dz_1 g(z_1) h(z - z_1) \equiv g \star h$ . Note that  $n_\nu^{(s)}$ ,  $\mathbf{n}_i^{(s)}$ , and  $n_\tau^{(p)}$  are weighted densities which involve only variables of either species, while  $n^{(sp)}$  is a convolution of the sphere density with an orientation-dependent weight function, combining characteristics of both species. The weight functions of the Rosenfeld excess free energy den-

sity read

$$w_0^{(s)}(z) = \frac{\Theta(R_s - |z|)}{2R_s}, \quad (10)$$

$$w_1^{(s)}(z) = \frac{\Theta(R_s - |z|)}{2} = \frac{w_2^{(s)}(z)}{4\pi R_s}, \quad (11)$$

$$w_3^{(s)}(z) = \pi(R_s^2 - z^2)\Theta(R_s - |z|), \quad (12)$$

$$\mathbf{w}_1^{(s)}(z) = \frac{z\Theta(R_s - |z|)\mathbf{e}_z}{2R_s} = \frac{\mathbf{w}_2^{(s)}(z)}{4\pi R_s}, \quad (13)$$

where  $\mathbf{e}_z$  is the unit vector pointing along the  $z$  axis and  $\Theta(z)$  is the Heaviside step function. The Mayer function  $f_{ss}(z)$  of the interaction potential between two hard spheres is obtained through

$$-\frac{f_{ss}(z)}{2} = w_0^{(s)} \star w_3^{(s)} + w_1^{(s)} \star w_2^{(s)} - \mathbf{w}_1^{(s)} \star \mathbf{w}_2^{(s)}. \quad (14)$$

The Mayer function equals  $-1$  if the spheres intersect or touch each other and is zero otherwise. The remaining weight functions can be expressed as (see discussion below)

$$w_0^{(p)}(z, \theta_p) = \frac{\delta(R_p \sin \theta_p - |z|)}{2}, \quad (15)$$

$$w_1^{(p)}(z, \theta_p) = \frac{\pi\Theta(R_p \sin \theta_p - |z|)}{8 \sin \theta_p} = \frac{w_2^{(p)}(z, \theta_p)}{8R_p}, \quad (16)$$

and

$$w^{(sp)}(z, \theta_p) = \begin{cases} 8\sqrt{R_s^2 \cos^2 \theta_p - z^2} \\ + 8z \left[ \arcsin \left( \frac{z \tan \theta_p}{\sqrt{R_s^2 - z^2}} \right) \right] \sin \theta_p, \\ |z| < R_s \cos \theta_p \\ 4\pi|z| \sin \theta_p, \quad R_s \cos \theta_p \leq |z| \leq R_s. \end{cases} \quad (17)$$

These weight functions allow one to generate the Mayer function  $f_{sp}(z)$  of the interaction potential between a hard sphere and a thin platelet through

$$-f_{sp}(z, \theta_p) = w_0^{(p)} \star w_3^{(s)} + w_1^{(p)} \star w_2^{(sp)} + w_1^{(s)} \star w_2^{(p)}. \quad (18)$$

Equations (1) - (18) completely specify the density functional theory for the system under consideration.

Before studying the binary mixture of spheres and thin platelets in the bulk and near a hard wall it is instructive to compare the fundamental measure theory with the one which has been developed recently for a mixture of hard spheres and thin rods [13, 14, 15, 16]. For thin rods of length  $L$  the weight functions corresponding to Eqs. (15) - (17) are given by

$$w_0^{(r)}(z, \theta_r) = \frac{\delta\left(\frac{L}{2} \cos \theta_r - |z|\right)}{2}, \quad (19)$$

$$w_1^{(r)}(z, \theta_r) = \frac{\Theta\left(\frac{L}{2} \cos \theta_r - |z|\right)}{4 \cos \theta_r}, \quad (20)$$

$$w_2^{(r)}(z, \theta_r) = 0, \quad (21)$$

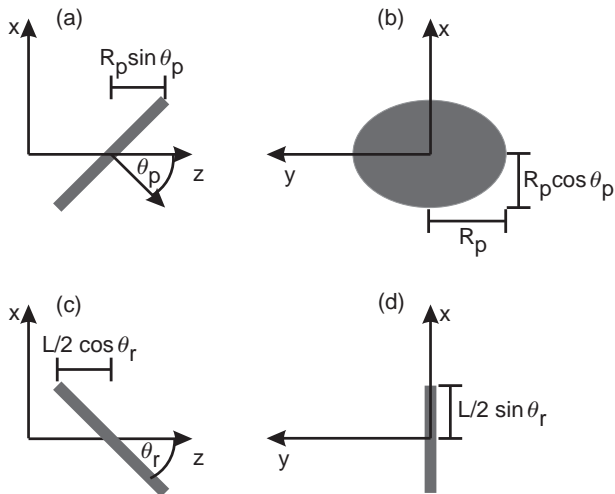


FIG. 1: Geometries relevant for the determination of the weight functions [Eqs. (15), (16), and (19) - (21)] for thin circular platelets of radius  $R_p$  [(a), (b)] and thin rods of length  $L$  [(c), (d)]. The angle between the normal of a platelet and the  $z$ -axis is denoted by  $\theta_p$  while the angle  $\theta_r$  characterizes the orientation of a rod with respect to the  $z$ -axis. Only the projections of the platelets and rods on the planes of the figures are shown.

and

$$w^{(sr)}(z, \theta_r) = \begin{cases} 8\sqrt{R_s^2 \sin^2 \theta_r - z^2} \\ + 8z \left[ \arcsin \left( \frac{z \cot \theta_r}{\sqrt{R_s^2 - z^2}} \right) \right] \cos \theta_r, \\ |z| < R_s \sin \theta_r \\ 4\pi|z| \cos \theta_r, & R_s \sin \theta_r \leq |z| \leq R_s. \end{cases} \quad (22)$$

Here  $\theta_r$  is the angle between the rod and the  $z$  axis (see Fig. 1). The Mayer function  $f_{sr}(z)$  of the interaction potential between a hard sphere and a thin rod is generated through

$$-f_{sr}(z, \theta_r) = w_0^{(r)} \star w_3^{(s)} + w_1^{(r)} \star w_2^{(sr)}. \quad (23)$$

The weight functions are linked with a geometrical representation of the particles which is given in terms of fundamental measures defined as  $\zeta_\lambda^{(j)} = \int dz w_\lambda^{(j)}$ , where  $j = s, p, r$  labels the species, and  $\lambda = 0, 1, 2, 3$  corresponds to the Euler characteristic, integral mean curvature, surface, and volume [20] of the particles. For spheres  $\zeta_0^{(s)} = 1$ ,  $\zeta_1^{(s)} = R_s$ ,  $\zeta_2^{(s)} = 4\pi R_s^2$ , and  $\zeta_3^{(s)} = 4\pi R_s^3/3$ , whereas for thin platelets the volume is very small and  $\zeta_0^{(p)} = 1$ ,  $\zeta_1^{(p)} = \pi R_p/4$ , and  $\zeta_2^{(p)} = 2\pi R_p^2$ . In the case of thin rods both the volume and the surface area are very small and  $\zeta_0^{(r)} = 1$ ,  $\zeta_1^{(r)} = L/4$ . For comparison we note that the integral mean curvature of a particle can be obtained from the general relation  $\zeta_1 = \int d\sigma (1/R_1 + 1/R_2)/(8\pi)$ , where  $R_1$  and  $R_2$  are the principle radii of curvature at the point  $\sigma$  on the surface and  $d\sigma$  is a surface element. The

evaluation of this integral is trivial for thin rods and is documented for thin platelets in the appendix of Ref. [21].

From their side view, platelets may be regarded as rods (see Figs. 1 (a) and (c)) and from their top view (in the direction of the normal to face) as two-dimensional spheres. Therefore the functional forms of the weight functions  $w_0^{(p)}(z)$ ,  $w_0^{(r)}(z)$  [Eqs. (15) and (19)] and  $w_1^{(p)}(z)$ ,  $w_1^{(r)}(z)$  [Eqs. (16) and (20)] are similar, while the weight function  $w_2^{(p)}(z)$  [Eq. (16)] takes into account the surface of the platelets (see Fig. 1 (b)).

In order to express the sphere-platelet and sphere-rod Mayer functions [Eqs. (18) and (23)] in terms of spatial convolution decompositions, additional weight functions  $w^{(sp)}(z, \theta_p)$  and  $w^{(sr)}(z, \theta_r)$  have to be introduced. These weight functions contain informations about both species of the binary mixtures. Since the explicit expression for the additional weight function [Eq. (22)] for the sphere-rod mixture is amply discussed in Ref. [16] we do not document the derivation of the expression for the corresponding weight function  $w^{(sp)}(z, \theta_p)$  [Eq. (17)] for the sphere-platelet mixture but analyze the cases  $\theta_p = 0$  and  $\theta_r = \pi/2$  in more detail. In these limits the weight functions reduce to  $w^{(sp)}(z, \theta_p = 0) = w^{(sr)}(z, \theta_r = \pi/2) = 8\sqrt{R_s^2 - z^2} \Theta(R_s - |z|)$ . Figure 2 displays schematic illustrations of the support of the sphere-platelet and sphere-rod Mayer functions which can be calculated analytically from Eqs. (18) and (23):

$$-f_{sp}(z, \theta_p = 0) = A_{sp}(z) \Theta(R_s - |z|), \quad (24)$$

$$A_{sp}(z) = \pi \left( \sqrt{R_s^2 - z^2} + R_p \right)^2, \quad (25)$$

and

$$-f_{sr}(z, \theta_r = \pi/2) = A_{sr}(z) \Theta(R_s - |z|), \quad (26)$$

$$A_{sr}(z) = \pi(R_s^2 - z^2) + 2L\sqrt{R_s^2 - z^2}. \quad (27)$$

Due to the steric interaction, the center of mass of a platelet [rod] is excluded from an area in the  $x - y$  plane of size  $A_{sp}(z_{12})$  [ $A_{sr}(z_{12})$ ] surrounding a sphere, where  $z_{12}$  is the distance along the  $z$  axis between the center of mass of the platelet [rod] and the sphere. Moreover it is apparent from the figure that the radius  $\sqrt{R_s^2 - z^2}$  and hence the weight function  $w^{(sp)}(z, 0)$  [ $w^{(sr)}(z, \pi/2)$ ] are characteristic of how a sphere looks from the viewpoint of a platelet [rod].

### III. BULK PHASE DIAGRAM

Based on the density functional given by Eqs. (1) - (18) and as a prerequisite for our wall-liquid interface study we first study the homogeneous bulk fluid with  $V_{ext,s}(\mathbf{r}) = 0$  and  $V_{ext,p}(\mathbf{r}, \omega_p) = 0$  in a macroscopic volume  $V$ . In this case the equilibrium density profiles are constant [ $\rho_s(\mathbf{r}) = \rho_s$  and  $\rho_p(\mathbf{r}, \omega_p) = \rho_p$ ] and the Euler-Lagrange equations resulting from the stationary conditions are

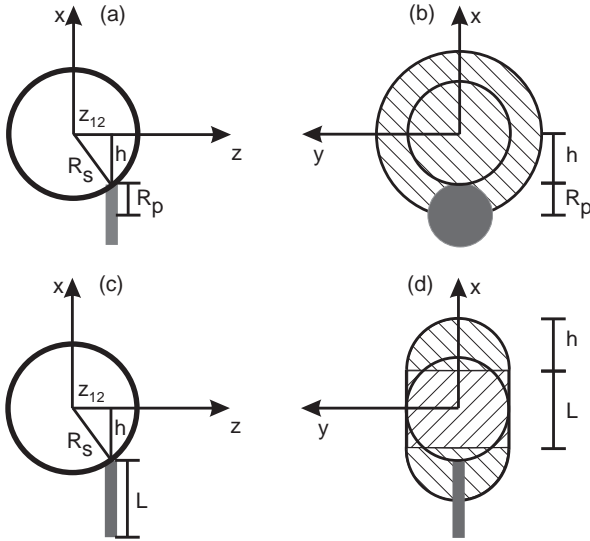


FIG. 2: Illustrations of the steric interactions of hard spheres with thin hard platelets and rods. (a) [(c)] Schematic side view of a sphere of radius  $R_s$  and a platelet of radius  $R_p$  [rod of length  $L$ ]. The normal of the platelet is parallel to the  $z$ -axis while the rod is oriented parallel to the  $x$ -axis. Only the projections of the particles on the planes of the figures are shown. (b) [(d)] Due to the steric interaction, the center of mass of the platelet [rod] is excluded from the hatched region surrounding the sphere in the  $x-y$  plane. Here the planes of the figures are located at  $z = z_{12}$ . From these figures the area  $A_{sp}(z_{12}) = \pi(h + R_p)^2$  [ $A_{sr}(z_{12}) = \pi h^2 + 2Lh$ ] with  $h = \sqrt{R_s^2 - z_{12}^2}$  can be inferred (see Eq. (25) [(27)]).

given by  $\partial\Omega[\rho_s, \rho_p]/\partial\rho_s = 0$  and  $\partial\Omega[\rho_s, \rho_p]/\partial\rho_p = 0$ . In the present study we restrict our attention to platelet number densities  $\rho_p R_p^3 \leq 0.2$  for which the pure platelet fluid and also the mixture are in the isotropic phase and hence  $\rho_s$  is independent of the orientation of the platelets. For comparison, the isotropic-nematic phase transition of the pure platelet fluid is first order with coexistence densities  $\rho_{pI} R_p^3 = 0.46$  and  $\rho_{pN} R_p^3 = 0.5$  according to a computer simulation [21]. The excess free energy density per volume can be expressed as

$$\frac{F_{ex}}{k_B T V} = \Phi_{s,b} - \rho_p \ln \alpha, \quad (28)$$

with

$$\frac{\alpha}{1 - \eta_s} = \exp \left( - \frac{(\pi^2 R_s^2 R_p + 2\pi R_p^2 R_s) \rho_s}{1 - \eta_s} - \frac{\pi^4 R_s^4 R_p^2 \rho_s^2}{2(1 - \eta_s)^2} \right), \quad (29)$$

where  $\eta_s = 4\pi R_s^3 \rho_s / 3$  is the packing fraction of the spheres and  $\Phi_{s,b}$  is the excess free energy density of a pure hard-sphere fluid.  $\alpha$  can be considered as the free-volume fraction, i.e., the relative amount of the volume

$V$  that is accessible to the platelets. Besides providing access to inhomogeneous density distributions the above geometry-based density functional theory for mixtures of hard spheres and platelets offers in addition a systematic approach to calculate the work  $W = -k_B T \ln \alpha$  required to insert a platelet into a solution of spheres. The expression for the free-volume fraction  $\alpha$  in Eq. (29) is equivalent to the result from a recent scaled-particle approach [10]. For comparison we note that the corresponding free-volume fraction for thin rods is given by

$$\frac{\alpha}{1 - \eta_s} = \exp \left( - \frac{\pi L R_s^2 \rho_s}{1 - \eta_s} \right). \quad (30)$$

From the bulk grand potential function all thermodynamic quantities can be calculated. Equating the pressure and the chemical potentials of both species in both phases yields the coexisting densities.

Figure 3 (a) displays the calculated phase diagram for a binary mixture of spheres and thin platelets for size ratio  $R_s/R_p = 8/3$  as a function of the chemical potential  $\mu_p$  of the platelets and the number density  $\rho_s$  of the spheres. The tie-lines are horizontal because of the equality of  $\mu_p$  of the coexisting phases. The binodal for coexisting states is shown, where a sphere-rich and a platelet-poor liquid phase coexists with a sphere-poor and a platelet-rich liquid phase. The coexistence region is bounded by a lower critical point below which only a single stable phase is found. For convenience we have introduced the dimensionless variable  $\mu_p^* \equiv \mu_p - k_B T \ln(\Lambda_p^3/R_p^3)$ , and dropped the star in order to avoid a clumsy notation. Figure 3 (b) displays an alternative representation of the phase diagram in terms of the number densities of both species. The figure illustrates the fractionation of both spheres and platelets due to the phase transition. Upon increasing the size ratio the critical point shifts to larger densities of the spheres.

The dotted lines in Fig. 3 represent the binodal as calculated without the term proportional to  $\rho_s^2$  in parenthesis on the r.h.s. of Eq. (29) which is equivalent to considering a binary mixture of spheres and thin rods of length  $L = \pi R_p + 2R_p^2/R_s = 1.46 R_s$  as is apparent from a comparison of Eqs. (29) and (30). The phase boundaries and the lower critical point are shifted to smaller values of  $\rho_s$ . In other words, the number density of the spheres in the sphere-poor phase is increased by taking into account the last term in parenthesis in Eq. (29).

#### IV. BINARY SPHERE-PLATELET MIXTURE NEAR A PLANAR HARD WALL

The density profiles of both components of the binary mixture of hard spheres and thin platelets close to a planar hard wall are obtained by a numerical minimization of the grand potential functional (1) with the excess free energy functional given by Eq. (2). We fix the chemical potential  $\mu_p$  of the platelets and approach the bulk phase

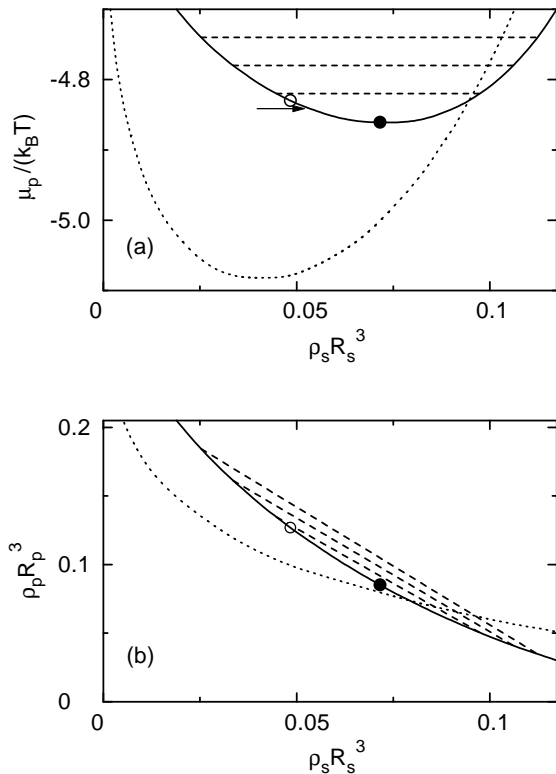


FIG. 3: (a) Bulk and surface phase diagrams of binary mixtures of hard spheres of radius  $R_s$  and thin hard platelets of radius  $R_p = 3R_s/8$  as a function of the chemical potential of the platelets  $\mu_p$  and the number density of the spheres  $\rho_s$ . The straight dashed lines are tie-lines illustrating liquid-liquid phase coexistence. (b) Phase diagram of the same fluid in the density-density plane, where  $\rho_p$  is the number density of the platelets. In (a) and (b) the solid and open circles denote the bulk critical point and the wetting transition point, respectively. Between the wetting transition point and the critical point the sphere-rich liquid phase completely wets the interface between the hard wall and the sphere-poor liquid phase. The dotted curve is the binodal as calculated without the last term in parenthesis on the r.h.s. of Eq. (29) which is equivalent to the bulk phase diagram of a binary mixture of spheres of radius  $R_s$  and thin rods of length  $L = 1.46 R_s$  [see the main text]. In Fig. 4 density profiles near a hard wall are shown along the thermodynamic path indicated by the arrow at  $\mu_p/(k_B T) = -4.85$  in (a); in (b) this path would run parallel to the dashed tie-lines.

boundary from the sphere-poor side. Upon decreasing  $\mu_p$  the adsorption behavior changes qualitatively, and it is worthwhile to distinguish the following two cases. For  $\mu_p/(k_B T) > -4.84$  we find that the wall is only partially wet by the spheres. The layer thickness of the sphere-rich phase forming close to the wall increases continuously, but remains finite at coexistence. For  $\mu_p/(k_B T) < -4.84$  we observe complete wetting. The transition to complete wetting appears to be first order because the excess adsorptions  $\Gamma_l = R_l^2 \int_0^\infty dz (\rho_l(z) - \rho_l(\infty))$  with  $l = p, r$ ,

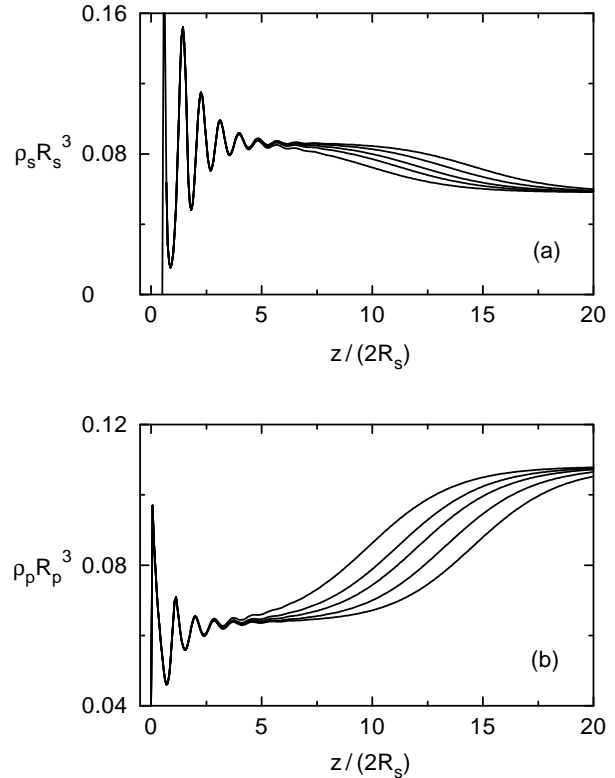


FIG. 4: Equilibrium density profiles of hard spheres of radius  $R_s$  (a) and thin hard platelets of radius  $R_p = 3R_s/8$  (b) in contact with a planar hard wall at  $z = 0$  as the bulk phase boundary is approached along the path indicated by the arrow in Fig. 3 (a). The chemical potentials of the spheres are  $\mu_s/(k_B T) = 25.82862, 25.82866, 25.8287, 25.82874, 25.82877$  corresponding to  $\rho_s R_s^3 = 0.058057, 0.058069, 0.058082, 0.058094, 0.058104$  (from left to right) where the chemical potential at bulk coexistence is  $\mu_s/(k_B T) = 25.8287774$  so that  $\rho_s R_s^3 = 0.058107$ . In (a)  $\rho_s(z < R_s) = 0$  and in (b)  $\rho_p(z < 0) = 0$ ; the contact values at  $z = R_s$  and  $z = 0$ , respectively, are not shown on the present scales.

calculated along the coexistence curve jump to a macroscopic value upon approaching the wetting transition point. Figure 4 (a) displays the sphere density profiles at  $\mu_p/(k_B T) = -4.85$  signalling the growth of a thick layer of sphere liquid at the wall. The corresponding platelet profiles are shown in Fig. 4 (b) and indicate how the platelets become more depleted as the sphere-rich layer grows. Upon approaching the chemical potential of the spheres at bulk coexistence  $\mu_s/(k_B T) = 25.8287774$ , the calculated density profiles at the liquid-liquid interface become virtually indistinguishable from the ones of the free liquid-liquid interface between coexisting bulk phases, and the layer thickness diverges logarithmically, as expected for the case of complete wetting in systems governed by short-ranged forces. With increasing chemical potential of the platelets, and hence increasing distance to the critical point [see Fig. 3 (a)], the interface

becomes sharper, i.e., it crosses over from one to the other limiting bulk value over a shorter distance. The wavelength  $\lambda = 1.72 R_s$  of the oscillations of the density profiles close to the wall reflects the size of the spheres.

Similar to recent studies of wetting in sphere-polymer [3, 5] and sphere-rod [4] mixtures, we have not been able to numerically resolve the prewetting line which should emerge tangentially from the coexistence curve at the wetting transition. In contrast to those studies there are no layering transitions in the partial wetting regime for the sphere-platelet mixture. This holds also for the aforementioned toy model without the last term in Eq. (4) which exhibits the same bulk phase diagram as the corresponding sphere-rod mixture (see the dotted curves in Fig. 3). Taking into account the weight function  $w_2^{(p)}(z, \theta_p)$  [Eq. (16)] leads to wetting phenomena of sphere-platelet mixtures which are different from those of sphere-rod mixtures even if the bulk phase diagrams of both systems are identical. Finally, we note that the wetting behavior discussed above remains unchanged upon increasing the size ratio of the platelets and the spheres (e.g.,  $R_p = R_s/2$ ).

## V. SUMMARY

We have developed a geometry-based density functional theory for fluids consisting of hard spheres and thin platelets. The bulk and surface phase diagram and the density profiles near a planar hard wall are determined numerically with the following main results.

(1) Figure 1 illustrates that from their side view thin platelets may be regarded as thin rods and from their top view as two-dimensional spheres. On the basis of this consideration we have shown that the geometry-based density functional theory developed for binary mixture of hard spheres and thin rods [13, 14, 15, 16] can be

consistently extended to the more challenging problem of hard spheres mixed with thin hard platelets by introducing an additional weight function which characterizes the surface of a platelet. The volume accessible to a thin platelet of radius  $R_p$  in the presence of a sphere is smaller than the corresponding one of a thin rod of length  $L = 2R_p$  because of the extended surface of the platelet (Fig. 2).

(2) The bulk phase diagram exhibits two-phase coexistence between sphere-rich and sphere-poor phases which is bounded by a lower critical point below which a single stable phase is found (Fig. 3). The phase boundaries and the critical point of the corresponding phase diagram for a binary mixture of hard spheres and thin rods are shifted to smaller values of the density of the spheres due to smaller intermolecular interactions between thin rods and spheres as compared with those between thin platelets and spheres.

(3) For the mixture near a planar hard wall, a first-order wetting transition by the sphere-rich phase occurs. In the partial wetting regime no layering transitions are found in contrast to recent studies on binary mixtures of spheres and non-adsorbing polymers or thin hard rods.

We have focused on the case of non-interacting platelets as regards their mutual interactions, which constitutes a minimal model for non-spherical particles with non-vanishing surface area. With increasing density of the platelets, interactions between platelets must be included [22, 23]. The consistent treatment of these non-trivial platelet-platelet interactions within a geometry-based density functional theory remains as a challenge.

## Acknowledgments

The authors thank R. Roth for useful discussions.

- 
- [1] W. C. K. Poon, P. N. Pusey, and H. N. W. Lekkerkerker, *Phys. World* **9**, 27 (1996).
  - [2] M. Adams, Z. Dogic, S. L. Keller, and S. Fraden, *Nature* **393**, 349 (1998).
  - [3] J. M. Brader, R. Evans, M. Schmidt, and H. Löwen, *J. Phys.: Condens. Matter* **14**, L1 (2002).
  - [4] R. Roth, J. M. Brader, and M. Schmidt, *Europhys. Lett.* **63**, 549 (2003).
  - [5] M. Dijkstra and R. van Roij, *Phys. Rev. Lett.* **89**, 208303 (2002).
  - [6] M. Piech and J. Y. Walz, *J. Colloid Interface Sci.* **232**, 86 (2000).
  - [7] S. M. Oversteegen and H. N. W. Lekkerkerker, *Phys. Rev. E* **68**, 021404 (2003).
  - [8] L. Harnau and S. Dietrich, *Phys. Rev. E* **69**, 051501 (2004).
  - [9] S. M. Oversteegen and H. N. W. Lekkerkerker, *Physica A* **341**, 23 (2004).
  - [10] S. M. Oversteegen and H. N. W. Lekkerkerker, *J. Phys. Chem.* **120**, 2470 (2004).
  - [11] T. G. Manson, *Phys. Rev. E* **66**, 060402(R) (2002).
  - [12] G. C. Maitland, *Curr. Opin. Colloid Interface Sci.* **5**, 301 (2000).
  - [13] M. Schmidt, *Phys. Rev. E.* **63**, 050201 (2001).
  - [14] M. Schmidt and C. von Ferber, *Phys. Rev. E.* **64**, 051115 (2001).
  - [15] M. Schmidt and A. R. Denton, *Phys. Rev. E.* **65**, 021508 (2002).
  - [16] J. M. Brader, A. Esztermann, and M. Schmidt, *Phys. Rev. E* **66**, 031401 (2002).
  - [17] Y. Rosenfeld, *Phys. Rev. Lett.* **63**, 980 (1989).
  - [18] P. Tarazona, *Phys. Rev. Lett.* **84**, 694 (2000).
  - [19] R. Roth, R. Evans, A. Lang, and G. Kahl, *J. Phys.: Condens. Matter* **14**, 12063 (2002).
  - [20] Y. Rosenfeld, *Phys. Rev. E* **50**, R3318 (1994).
  - [21] M. A. Bates, *J. Chem. Phys.* **111**, 1732 (1999).

- [22] L. Harnau, D. Costa, and J.-P. Hansen, *Europhys. Lett.* **53**, 729 (2001). (2002).
- [23] L. Harnau and S. Dietrich, *Phys. Rev. E* **65**, 021505